Experimental Section

Synthesis of Sb_2S_3

All chemicals were used as received without further purification. Sb_2S_3 was prepared by a solvothermal method[1]. Briefly, 1 mmol $SbCl_3$ and 0.5 g L-cysteine were dissolved 30 mL ethylene glycol under stirring, followed by adjusting the suspension pH to 10 with NaOH (10 mol/L). Afterwards, the suspension was transferred into Teflon-lined stainless autoclave which is treated at 160 °C for 24 h. After cooling, the precipitates were collected and washed with deionized water/ethanol and then dried under vacuum.

Electrochemical experiments

Electrochemical measurements were carried out on a CHI-760E electrochemical work station using a three-electrode system consisting of Ag/AgCl (saturated KCl) electrode as the reference electrode, graphite rod as the counter electrode, and the catalyst coated on carbon cloth (CC) as the working electrode. All potentials were referenced to the reversible hydrogen electrode (RHE) on the basis of E_{RHE} (V)=$E_{Ag/AgCl}$+0.198+0.059×pH. The CC (1 × 1 cm^2) was pretreated by soaking it in 0.5 M H_2SO_4 for 12 h, and then washed with several times and dried at 60 °C for 24 h. To prepare the working electrode, 1 mg of catalyst was dispersed in 100 μl of mixed solvent containing 95 μL of ethanol and 5 μL of Nafion (5 wt%) by a continuous ultrasonication for about 1 h to generate a homogeneous ink. Then 50 μL of the dispersion was drop-casted onto the 1×1 cm^2 CC substrate and dried at room temperature. Electrochemical NORR tests were performed using a gas-tight H-type two-compartment electrochemical cell separated by a Nafion 211 membrane. The Nafion membrane was pretreated by boiling it in 5% H_2O_2 solution for 1 h, 0.5 M H_2SO_4 for 1 h and deionized water for 1 h in turn. Prior to NORR test, all feeding gases were purified through two glass bubblers containing 4 M KOH solution and the cathodic compartment was purged with Ar for at least 30 min to remove residual oxygen[2]. During the potentiostatic testing, NO flow (99.9%, 20 mL min^{-1}) was continuously fed to the cathodic compartment. After electrolysis for 1 h at various

potentials, liquid and gas products were detected by colorimetry and gas chromatography (GC, Shimadzu GC2010), respectively.

Determination of NH_3

The generated NH_3 was determined by the indophenol blue method[3]. Typically, 0.5 mL electrolyte was removed from the electrochemical reaction vessel and diluted 10 times with deionized water. Then 2 mL diluted solution was removed into a clean vessel followed by sequentially adding NaOH solution (2 mL, 1 M) containing $C_7H_6O_3$ (5 wt.%) and $C_6H_5Na_3O_7$ (5 wt.%), NaClO (1 mL, 0.05 M), and $C_5FeN_6Na_2O$ (0.2 mL, 1wt.%) aqueous solution. After the incubation for 2 h at room temperature, the mixed solution was subjected to UV-vis measurement using the absorbance at 655 nm wavelength.

The detailed procedures for colorimetric determination of N_2H_4 is provided in our previous publications[4]

Calculations of NH_3 yield rate and FE_{NH3}

$$\mathrm{NH_3\ yield\ rate}\ (\mu\mathrm{g\ h^{-1}\ cm^{-2}}) = \frac{c_{\mathrm{NH_3}} \times V}{t \times A} \quad (1)$$

$$\mathrm{FE_{NH3}}\ (\%) = \frac{5 \times F \times c_{\mathrm{NH_3}} \times V}{17 \times Q} \times 100\% \quad (2)$$

where c_{NH3} (μg mL^{-1}) is the measured NH_3 concentration, V (mL) is the volume of the electrolyte, t (h) is the reduction time, A (cm^{-2}) is the surface area of CC (1×1 cm^2) , F (96500 C mol^{-1}) is the Faraday constant, Q (C) is the quantity of applied electricity.

Characterizations

X-ray diffraction (XRD) pattern was collected on a Rigaku D/max 2400 diffractometer. Transmission electron microscopy (TEM) and high-resolution transmission electron microscopy (HRTEM) were recorded on a Tecnai G^2 F20 microscope. X-ray photoelectron spectroscopy (XPS) analysis was conducted on a PHI 5702 spectrometer. Nitrogen adsorption/desorption isotherms were performed on an ASAP 2020 instrument. The UV-vis absorbance measurements were performed on a MAPADA P5 spectrophotometer. On-line differential electrochemical mass spectrometry (DEMS, QAS 100) was carried out on a by QAS

100 spectrometer. The CC-supported catalyst, platinum wire, and Ag/AgCl electrodes were adopted as the working, counter, and reference electrodes, respectively. The various products during the electrolysis reactions were monitored at different values of *m*/*z* ionic signals.

Calculation details

DFT calculations were performed using the Cambridge sequential total energy package (CASTEP) with projector augmented wave pseudopotentials. The Perdew-Burke-Ernzerhof (PBE) generalized gradient approximation (GGA) functional was used for the exchange-correlation potential. DFT-D method was employed to calculate the van der Waals (vdW) interaction. The calculations were performed using a plane-wave cutoff energy of 550 eV, and a Monkhorst-Pack grid (3 × 3 × 1) was used for k-point sampling. Besides, the convergence thresholds of energy and forces were set to be 1.0×10^{-5} eV and 0.02 eV $Å^{-1}$, respectively. Sb_2S_3 (130) was modeled by a 2 × 1 supercell, and a vacuum region of 15 Å was used to separate adjacent slabs.

The free energies (ΔG, 298 K) for each reaction were given after correction:

$$\Delta G=\Delta E+\Delta ZPE-T\Delta S \tag{3}$$

where ΔE is the adsorption energy, ΔZPE is the zero-point energy difference and $T\Delta S$ is the entropy difference between the gas phase and adsorbed state.

MD simulations were carried out using a force field type of universal. The electrolyte system was modeled by a cubic cell with placing catalyst at the center of the cell and randomly filling 1000 H_2O, 50 NO, and 50 H. After geometry optimization, the MD simulations were performed in an NVT ensemble (298 K) with the total simulation time of 1 ns at a time step of 1 fs.

The radial distribution function (RDF) is calculated as

$$\mathrm{g(r)}=\frac{dN}{4\pi\rho r^2 dr} \tag{4}$$

where dN is the amount of NO in the shell between the central particle r and $r+dr$, ρ is the number density of NO, H_2O, and H.

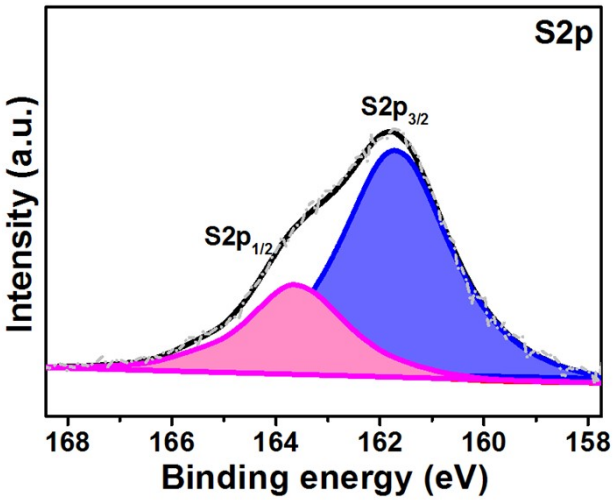

Fig. S1. XPS S2p spectrum of S_2S_3.

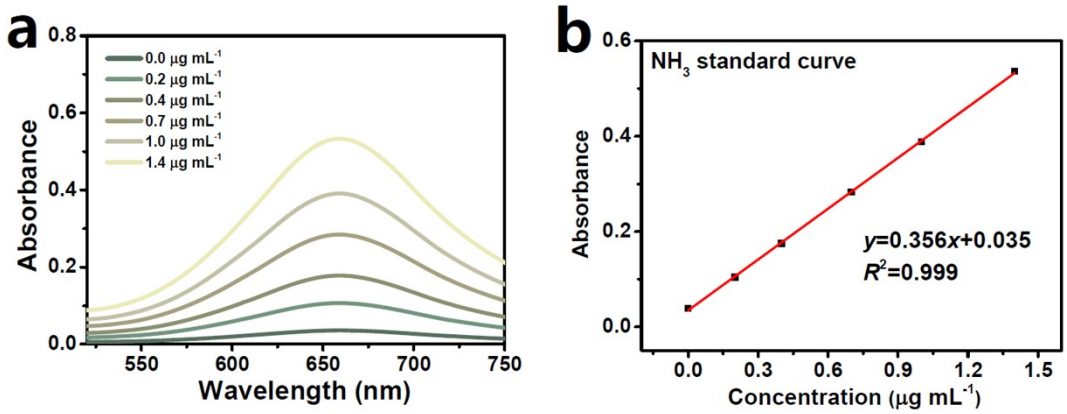

Fig. S2. (a) UV-vis absorption spectra of NH_4^+ assays after incubated for 2 h at ambient conditions. (b) Calibration curve used for the calculation of NH_3 concentrations.

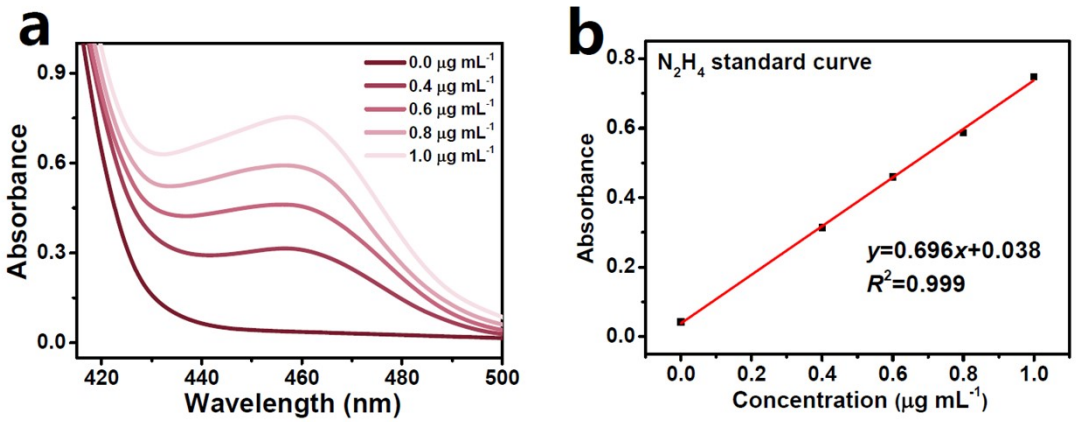

Fig. S3. (a) UV-vis absorption spectra of N_2H_4 assays after incubated for 20 min at ambient conditions. (b) Calibration curve used for calculation of N_2H_4 concentrations.

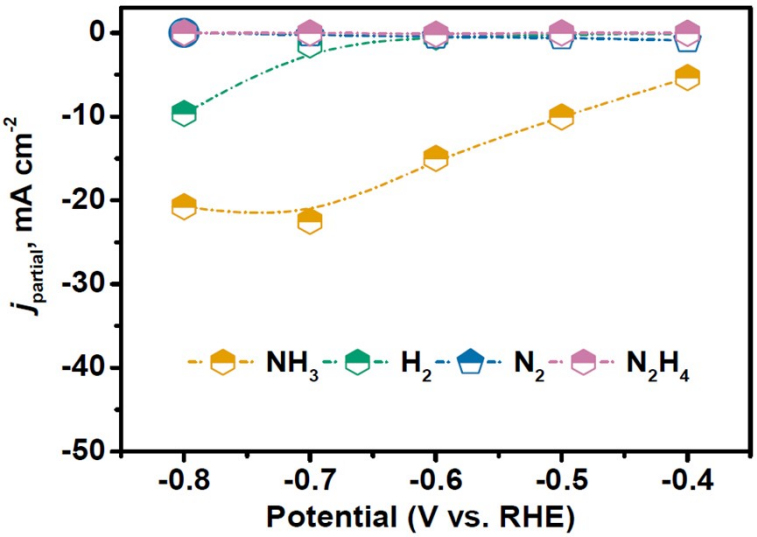

Fig. S4. Partial current densities of various products over Sb_2S_3 after 1 h of NORR electrolysis at different potentials.

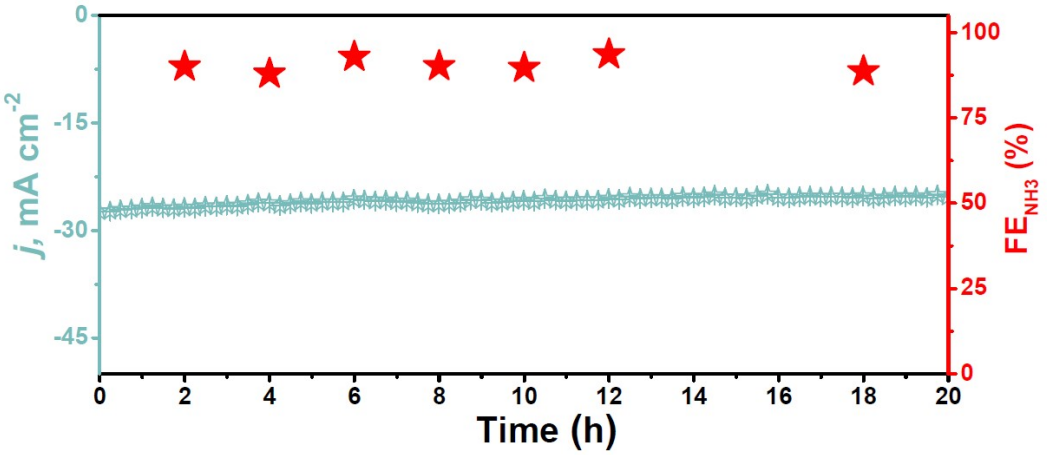

Fig. S5. Chronopotentiometric test of Sb_2S_3 for 20 h at -0.7 V.

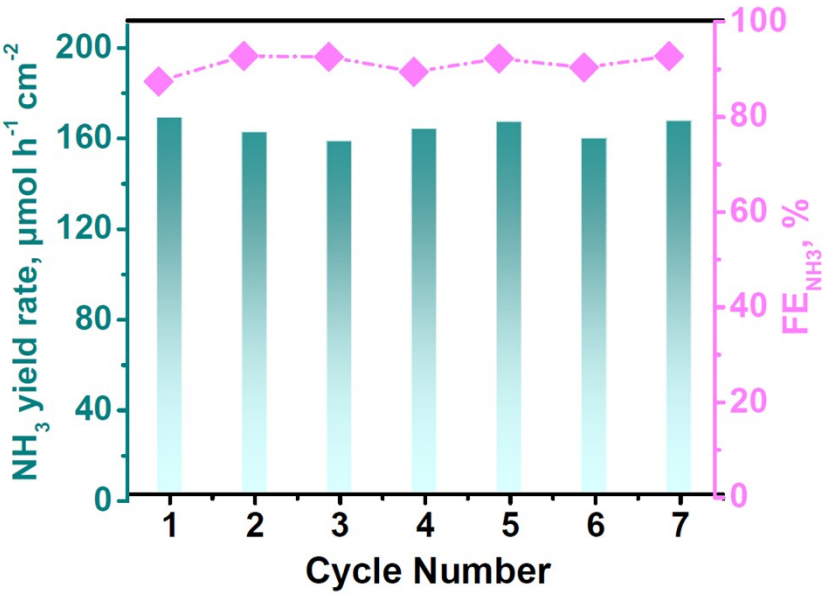

Fig. S6. Cycling test of Sb_2S_3 at -0.7 V.

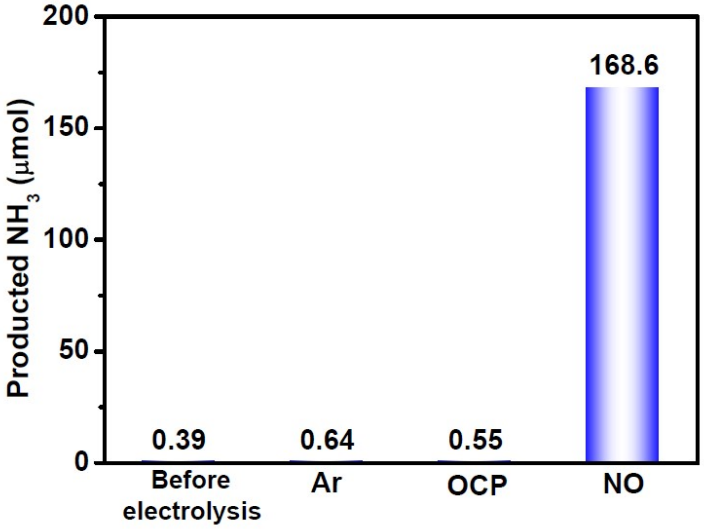

Fig. S7. Amounts of produced NH_3 on Sb_2S_3 under different conditions. (1) before electrolysis; (2) electrolysis in Ar-solution at -0.7 V; (3) electrolysis in NO-solution at open-circuit potential (OCP); (4) electrolysis in NO-solution at -0.7 V.

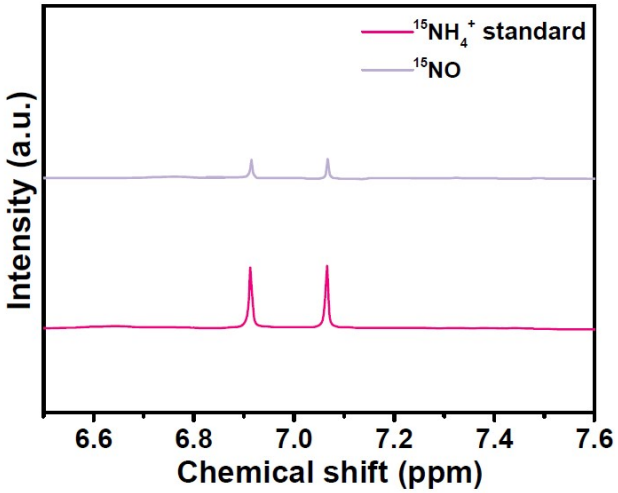

Fig. S8. ^{1}H NMR spectra of $^{15}NH_4^+$ standard sample and those fed by ^{15}NO and Ar after NORR electrolysis on Sb_2S_3 at -0.7 V.

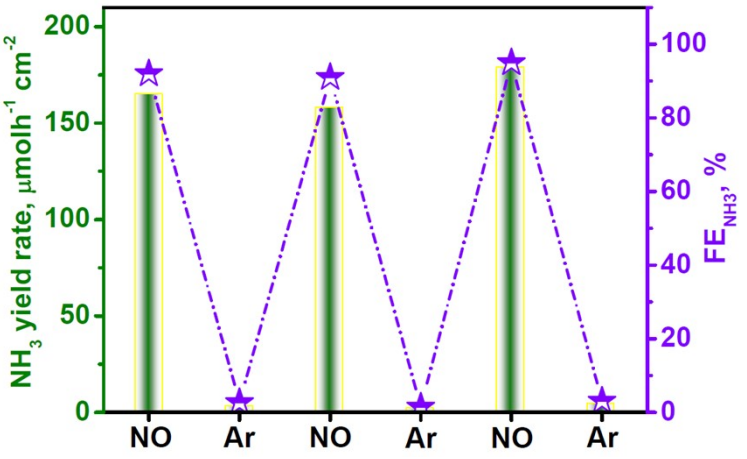

Fig. S9. NO-Ar switching test on Sb_2S_3 at -0.7 V.

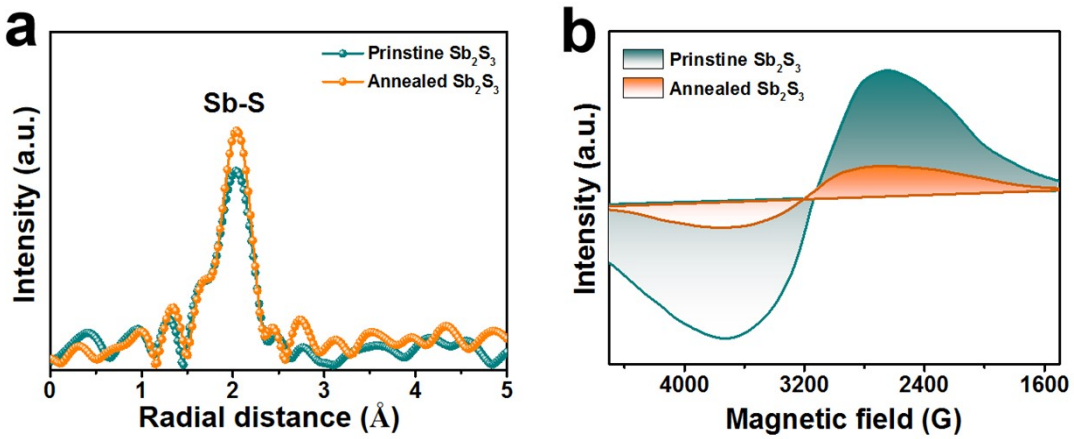

Fig. S10. (a) Sb K-edge EXAFS spectra and (b) EPR spectra of pristine Sb_2S_3 and a-Sb_2S_3.

Anneal Sb_2S_3 (defined as a-Sb_2S_3) was prepared by annealing pristine Sb_2S_3 in sulfur vapor at 500 °C for 2 h. It is shown in Fig. S10 that compared to pristine Sb_2S_3, a-Sb_2S_3 shows a much enhanced Sb-S bond intensity (Fig. S10a, Table S1) and reduced EPR intensity at g=2.002 (Fig. S10b), suggesting that pristine Sb_2S_3 contains abundant Sb_{AIU}, while Sb_{AIU} concentration is largely reduced after annealing treatment of Sb_2S_3 in sulfur vapor.

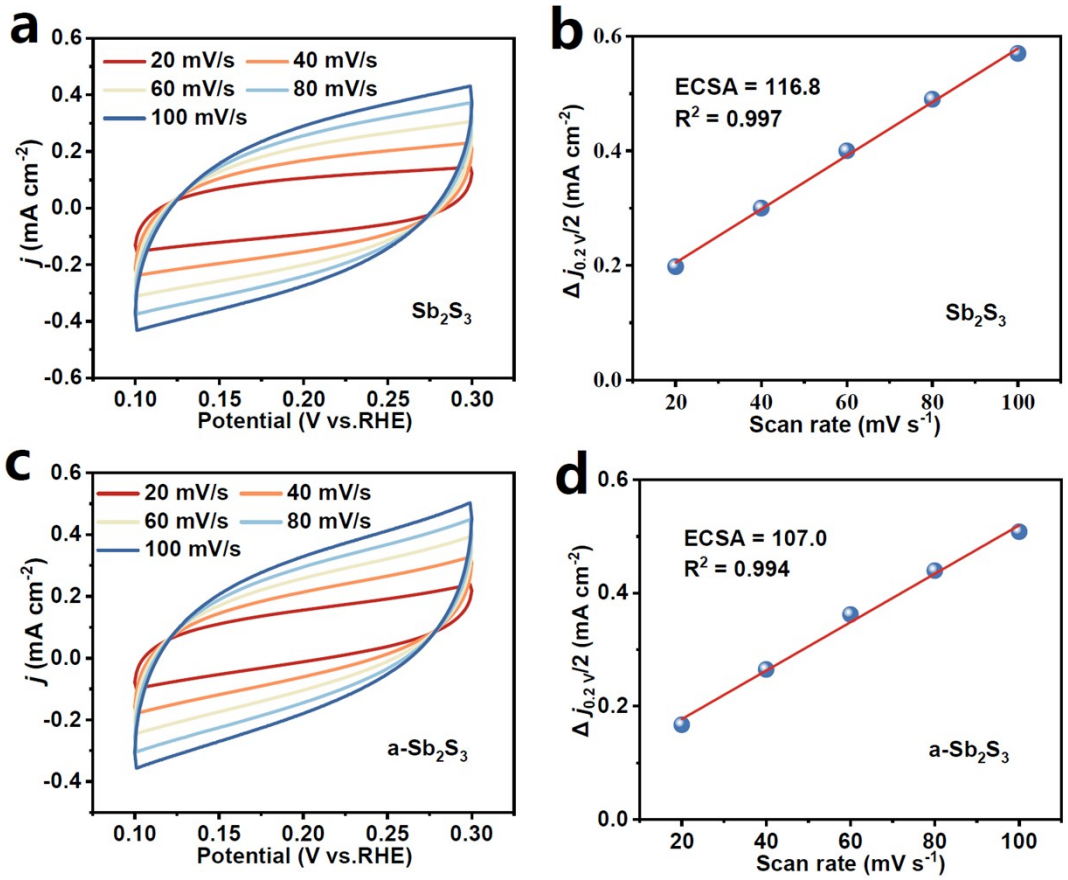

Fig. S11. CV measurements at different scanning rates and calculated ECSA for (a, b) Sb_2S_3 and (c, d) a-Sb_2S_3.

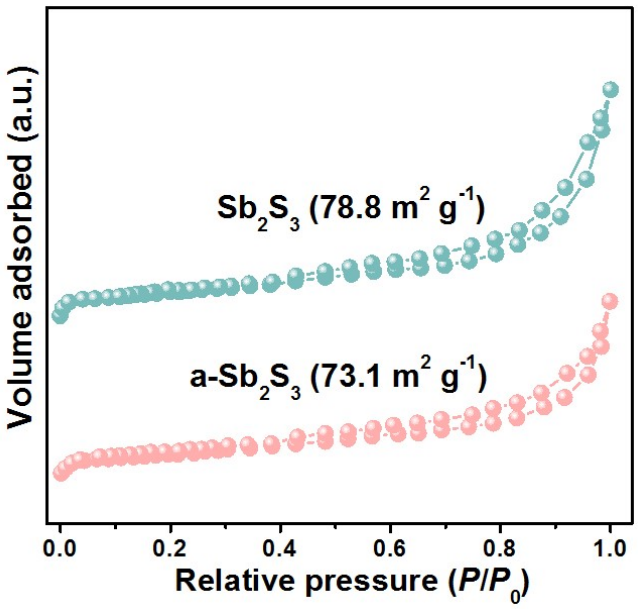

Fig. S12. Nitrogen adsorption/desorption isotherms of Sb_2S_3 and a-Sb_2S_3.

It is seen that the specific surface area of Sb_2S_3 (78.8 m^2 g^{-1}) is comparable to that of a-Sb_2S_3 (73.1 m^2 g^{-1}), consistent with the ECSA data (Fig. S11).

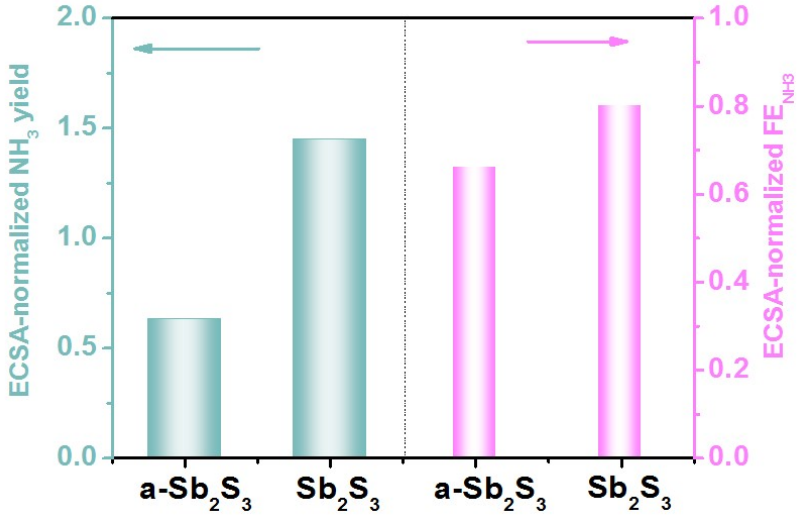

Fig. S13. ECSA-normalized NH_3 yield rates and FE_{NH3} of Sb_2S_3 and a-Sb_2S_3 at -0.7 V.

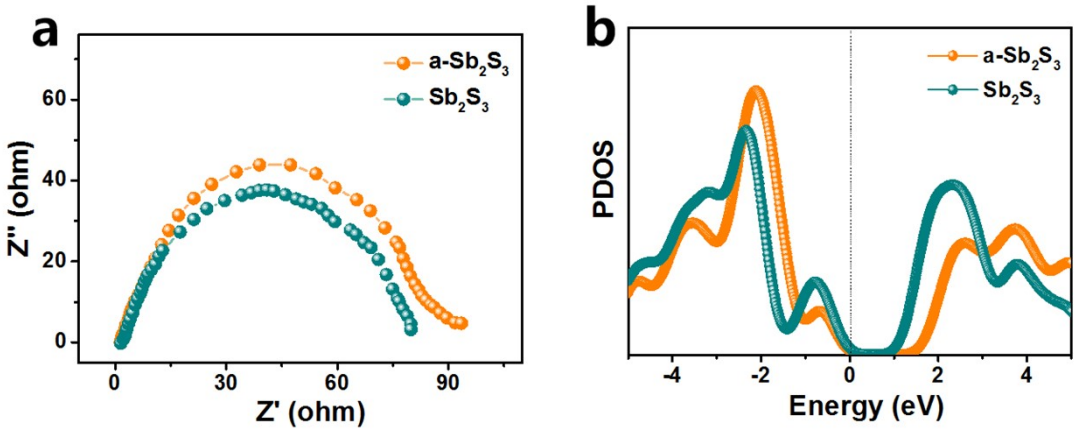

Fig. S14. (a) Electrochemical impendence spectra (EIS) of Sb_2S_3 and a-Sb_2S_3. (b) DOS profiles of Sb_2S_3 and a-Sb_2S_3.

It is seen in Fig. S14a that Sb_2S_3 exhibits a slightly reduced charge transfer resistance than a-Sb_2S_3, which is attributed to the Sb_{AIU}-induced narrowed band gap and enhanced conductivity of Sb_2S_3 compared to a-Sb_2S_3 (Fig. S14b).

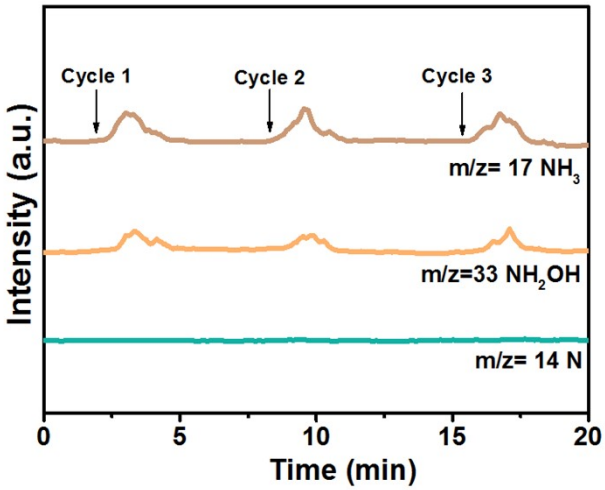

Fig. S15. Online DEMS spectra of Sb_2S_3 during the NORR electrolysis at -0.7 V.

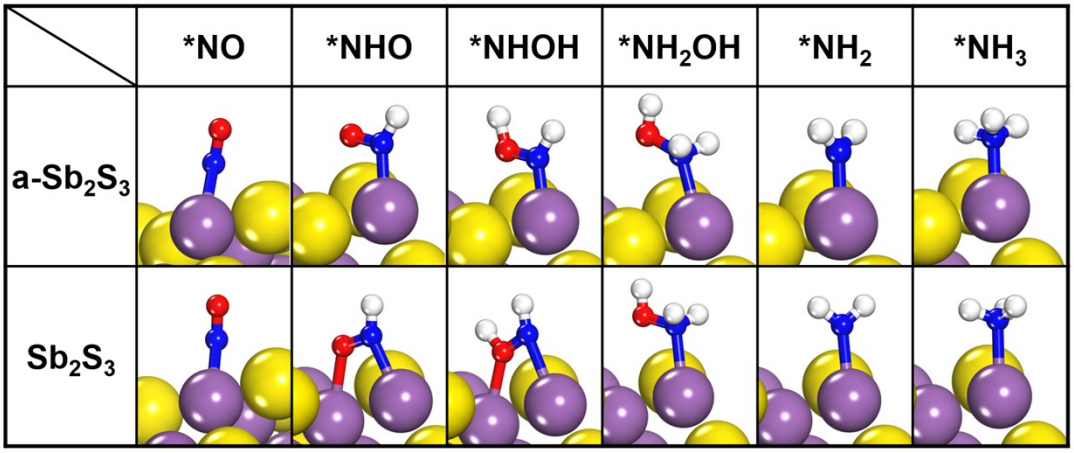

Fig. S16. Optimized structures of NORR intermediates on (a) a-Sb_2S_3 and (b) Sb_2S_3.

Table S1. Structural parameters extracted from the Sb K-edge EXAFS fitting.

Sample	Shell	CN	R (Å)	σ^2 (10^{-3}Å)	ΔE_0 (eV)	R factor (%)
Sb_2S_3	Sb-S	4.2	2.63	8.2	3.1	0.08
a-Sb_2S_3	Sb-S	4.8	2.61	5.1	2.2	0.1

Table S2. Comparison of the optimum NH_3 yield and NH_3-Faradic efficiency (FE_{NH3}) for recently reported state-of-the-art NORR electrocatalysts at ambient conditions.

Catalyst	Electrolyte	NH_3 yield rate ($\mu mol\ h^{-1}\ cm^{-2}$)	FE_{NH3} (%)	Potential (V vs. RHE)	Ref.
MoS_2/GF	0.1 M HCl	99.6	76.6	0.1	[5]
NiO/TM	0.1 M Na_2SO_4	125.3	90	-0.6	[6]
FeP/CC	0.2 M PBS	85.62	88.49	-0.2	[7]
Fe_1/MoS_{2-x}	0.5 M Na_2SO_4	288.2	82.5	-0.6	[8]
$Cu_2O@CoMN_2O_4$	0.1 M Na_2SO_4	94.18	75.05	-0.9	[9]
Ni_2P/CP	0.1 M HCl	33.47	76.9	-0.2	[10]
$Ru_{0.05}Cu_{0.95}$	0.05 M Na_2SO_4	17.68	64.9	-0.5	[11]
a-$B_{2.6}C@TiO_2$/Ti	0.1 M Na_2SO_4	216.4	87.6	-0.9	[12]
Ni@NC	0.1 M HCl	34.6	72.3	0.16	[13]
Bi NDs	0.1 M Na_2SO_4	70.2	89.2	-0.5	[14]
MoC/NCS	0.1 M HCl	79.4	89	-0.8	[15]
CoS_{1-x}	0.2 M Na_2SO_4	44.67	53.62	-0.4	[16]
Sb_2S_3	**0.5 M Na_2SO_4**	**168.6**	**93.7**	**-0.7**	**This work**

Supplementary references

[1]. H. Nan, Y. Liu, Q. Li, P. Shen and K. Chu, *Chem. Commun.*, 2020, **56**, 10345-10348

[2]. L. Zhang, J. Liang, Y. Wang, T. Mou, Y. Lin, L. Yue, T. Li, Q. Liu, Y. Luo, N. Li, B. Tang, Y. Liu, S. Gao, A. A. Alshehri, X. Guo, D. Ma and X. Sun, *Angew. Chem. Int. Edit.*, 2021, **60**, 25263-25268.

[3]. P. Li, Z. Jin, Z. Fang and G. Yu, *Energy Environ. Sci.*, 2021, **14**, 3522-3531.

[4]. Y. Luo, K. Chen, P. Shen, X. Li, X. Li, Y. Li and K. Chu, *J. Colloid Interf. Sci.*, 2023, **629**, 950-957.

[5]. L. Zhang, J. Liang, Y. Wang, T. Mou, Y. Lin, L. Yue, T. Li, Q. Liu, Y. Luo, N. Li, B. Tang, Y. Liu, S. Gao, A. A. Alshehri, X. Guo, D. Ma and X. Sun, *Angew. Chem. Int. Ed.*, 2021, **133**, 25467-25472.

[6]. P. Liu, J. Liang, J. Wang, L. Zhang, J. Li, L. Yue, Y. Ren, T. Li, Y. Luo, N. Li, B. Tang, Q. Liu, A. M. Asiri, Q. Kong and X. Sun, *Chem. Commun.*, 2021, **57**, 13562-13565.

[7]. J. Liang, Q. Zhou, T. Mou, H. Chen, L. Yue, Y. Luo, Q. Liu, M. S. Hamdy, A. A. Alshehri, F. Gong and X. Sun, *Nano Res.*, 2022, **15**, 4008-4013.

[8]. K. Chen, J. Wang, J. Kang, X. Lu, X. Zhao and K. Chu, *Appl. Catal. B*, 2023, **324**, 122241.

[9]. C. Bai, S. Fan, X. Li, Z. Niu, J. Wang, Z. Liu and D. Zhang, *Adv. Funct. Mater.*, 2022, **32**, 2205569.

[10]. T. Mou, J. Liang, Z. Ma, L. Zhang, Y. Lin, T. Li, Q. Liu, Y. Luo, Y. Liu, S. Gao, H. Zhao, A. M. Asiri, D. Ma and X. Sun, *J. Mater. Chem. A*, 2021, **9**, 24268-24275.

[11]. J. Shi, C. Wang, R. Yang, F. Chen, N. Meng, Y. Yu and B. Zhang, *Sci. China Chem.*, 2021, **64**, 1493-1497.

[12]. J. Liang, P. Liu, Q. Li, T. Li, L. Yue, Y. Luo, Q. Liu, N. Li, B. Tang, A. A. Alshehri, I. Shakir, P. O. Agboola, C. Sun and X. Sun, *Angew. Chem. Int. Ed.*, 2022, **61**, e202202087.

[13]. S. Sethuram Markandaraj, T. Muthusamy and S. Shanmugam, *J. Adv. Sci*, 2022, **9**, 2201410.

[14]. Y. Lin, J. Liang, H. Li, L. Zhang, T. Mou, T. Li, L. Yue, Y. Ji, Q. Liu, Y. Luo, N. Li, B. Tang, Q. Wu, M. S. Hamdy, D. Ma and X. Sun, *Mater. Today Phys.*, 2022, **22**.

[15]. G. Meng, M. Jin, T. Wei, Q. Liu, S. Zhang, X. Peng, J. Luo and X. Liu, *Nano Res.*, 2022, **15**, 8890-8896.

[16]. L. Zhang, Q. Zhou, J. Liang, L. Yue, T. Li, Y. Luo, Q. Liu, N. Li, B. Tang, F. Gong, X. Guo and X. Sun, *Inorg. Chem.*, 2022, **61**, 8096-8102.